Influence of the backflow effect on the orientational dynamics induced by light in nematics

D. O. Krimer,[1,*] G. Demeter,[2] and L. Kramer[1,†]
[1]*Physikalisches Institut der Universität Bayreuth, D-95440 Bayreuth, Germany*
[2]*Research Institute for Particle and Nuclear Physics of the Hungarian Academy of Sciences, H-1525 Budapest, P.O. Box 49, Hungary*
(Received 19 January 2005; published 16 May 2005)

We investigate the dynamical phenomena induced by a circularly polarized plane wave incident perpendicularly on a homeotropically aligned nematic layer. We study theoretically the influence of the velocity field (backflow effect) on the bifurcation scenario. Whereas backflow leads to substantial quantitative changes of secondary bifurcation thresholds, the overall bifurcation scenario remains unchanged. In the regime of uniform precession of the director with large reorientation, an unanticipated spatial oscillation of the flow field across the layer is found. Quantitative comparison with experimental large-aspect ratio systems is now possible.

DOI: 10.1103/PhysRevE.71.051711 PACS number(s): 42.70.Df, 42.65.Sf, 61.30.Gd

I. INTRODUCTION

Liquid crystals (LCs) demonstrate a rich variety of interesting optical phenomena which have been studied intensively during the past two decades. A nematic LC behaves optically as a uniaxial anisotropic medium with the optical axis along the local molecular orientation described by the director $\mathbf{n}(\mathbf{r},t)$ (note that $\mathbf{n}$ and $-\mathbf{n}$ are indistinguishable). Furthermore, when light propagates through the nematic, its electric field exerts a torque on the molecules which can induce molecular reorientation. The director reorientation leads to a change of the optical properties of the LC and, as a consequence, the light polarization is changed as it propagates through the layer. Such feedback between the light and the nematic gives rise to interesting nonlinear dynamical phenomena [1,2].

The first (primary) instability is the so-called light-induced Fréedericksz transition (LIFT), where the initial director alignment becomes unstable above a certain light intensity and the director reorients [1]. One of the most intriguing geometries is obtained when a circularly polarized light wave is incident perpendicularly on a thin, homeotropically aligned layer of nematic cell. (This is a thin layer of nematic liquid crystal sandwiched between two glass plates, whose surfaces have been treated so as to induce a perpendicular orientation of the nematic director at the glass-nematic interface.) In this case, the LIFT is observed to be weakly hysteretic, and above threshold the molecules undergo a collective rotation [3] that corresponds to a uniform precession of the director around the symmetry axis. This effect is well understood in the frame of a purely classical (hydrodynamic) approach [3]. It also can be interpreted in a quantum picture as spin angular momentum transfer from the light to the medium and is called self-induced stimulated light scattering [4].

In [5], a theoretical and experimental investigation of the dynamical behavior of the system for the region of higher intensities was reported. The authors of [5] observed a further discontinuous transition with large hysteresis from the precession regime with small reorientation amplitude occurring above the LIFT to one with large reorientation. The approximate model presented could describe qualitatively both regimes of uniform director precession. The frequency of the large-amplitude precession was found to be much smaller than the one just above the LIFT and to exhibit rapid variations with the incident intensity reaching zero at roughly periodic intervals. The authors presented clear experimental evidence of the frequency reduction in the second regime. The nature of the transition from one regime to the other was, however, not understood in the framework of this model.

More recently, Brasselet *et al.* [6,7], identified experimentally a new continuous transition from the small-amplitude uniform precession state to a more complex state with a precession-nutation type motion of the director. Recently, this intermediate regime and the nature of the transitions between the different states were successfully extracted from a theory involving the full director dynamics (but not the velocity field) [8,9].

However, quantitative differences with the experiment remain. In the experiment, the measured onset of the precession-nutation motion turns out to be about 20% lower than predicted by theory. Within the framework of the standard hydrodynamic description, one can think of two reasons for the discrepancy. One is that in the theory, a plane-wave approximation was used, whereas in the experiment, the transversal size of the laser beam was of the order of the thickness of the layer. Actually, the ratio δ between the diameter of the beam and the width of the layer is another bifurcation parameter (in the plane-wave approximation $\delta \to \infty$) and was shown to play a crucial role on the orientational dynamics [10]. The other reason is that in almost all theoretical treatments developed up to now, the velocity field induced by the director motion has been neglected. Indeed, director reorientation itself generates flow, even in the absence of external forces acting on the fluid. This is the so-called backflow effect. To calculate it, one has to include the equation for the velocity $\mathbf{v}$ and consider the coupled director-velocity equations in the framework of the well-established hydrodynamic approach [11]. To our knowledge, backflow was considered in the context of light-induced orientational

*Electronic address: Dmitry.Krimer@uni-bayreuth.de
†Deceased.

dynamics only in [12]. That treatment is restricted to small director reorientation where backflow can be included in a renormalized (reduced) orientational viscosity, which does not capture essential features. In Sec. III, we will make contact with this approximation.

The aim of this article is to clarify the influence of the backflow effect (at least in one particular geometry). Thereby, a full theory is developed starting from the nematodynamic equations, which eventually could be used for a quantitative comparison with experiment.

Rigorous treatments of backflow effects have been presented before in the context of electrically driven director dynamics in nematics. In particular, the Fréedericksz transition in twisted nematic cells [13,14], the backflow in the relaxation of a hybrid aligned nematic cells [15], and switch-on effects in hybrid aligned cells [16] were considered. It turns out that in these cases the backflow leads to qualitative changes of the director dynamics. Another interesting example (although in a different context) is the influence of the backflow in the problem of capillary waves at nematic-isotropic interfaces. In [17], the backflow was shown to play an important role on the dispersion relation of capillary waves.

The paper is organized as follows. In Sec. II, we present the theoretical framework of our problem by eliminating the flow field adiabatically. This theory can be applied also to systems where the director is reoriented by other torques (electric, magnetic,…). In Sec. III, we perform the linear stability analysis of the homeotropic state and show the influence of the backflow. The numerical method for calculating the dynamical regimes is described in Sec. IV. In Sec. V, we present the bifurcation scenario for our system and compare with the known scenario without backflow. Finally, our conclusions and perspectives are summarized in Sec. VI. Some expressions appearing in the velocity-eliminated director equations are listed in Appendix A. The equations for the light propagation in terms of the amplitudes for the ordinary and extraordinary waves are derived in Appendix B.

II. THEORY

A. Basic hydrodynamic equations

The Navier-Stokes equation for the velocity $\mathbf{v}$ can be written as [11]

$$\rho_m(\partial_t + \mathbf{v}\cdot\boldsymbol{\nabla})v_i = -\boldsymbol{\nabla}_j(p\delta_{ij} + \pi_{ij} + T_{ij}^{visc}), \tag{1}$$

where ρ_m and p are the density and the pressure of the LC, respectively. π_{ij} is the Ericksen stress tensor defined as

$$\pi_{ij} = \frac{\partial F}{\partial(\partial_j n_k)}\partial_i n_k \quad i = x,y,z, \tag{2}$$

where summation over doubly occurring indices is assumed. In Eq. (2), F is the free energy density which consists of the elastic part,

$$F^{(elast)} = \frac{K_1}{2}(\boldsymbol{\nabla}\cdot\mathbf{n})^2 + \frac{K_2}{2}(\mathbf{n}\cdot\boldsymbol{\nabla}\times\mathbf{n})^2 + \frac{K_3}{2}(\mathbf{n}\times\boldsymbol{\nabla}\times\mathbf{n})^2 \tag{3}$$

and the external part which is here

$$F^{(ext)} = -\frac{\varepsilon_a}{16\pi}|\mathbf{n}\cdot\mathbf{E}|^2. \tag{4}$$

Here K_1, K_2, and K_3 are, respectively, the splay, twist, and bend elastic constants [11] and $\mathbf{E}$ is the amplitude of the optical electric field. The viscous stress tensor T_{ij}^{visc} in Eq. (1) is written in terms of the six Leslie coefficients α_i [18],

$$-T_{ij}^{visc} = \alpha_1 n_i n_j n_k n_l A_{kl} + \alpha_2 n_j N_i + \alpha_3 n_i N_j + \alpha_4 A_{ij} + \alpha_5 n_j n_k A_{ki} + \alpha_6 n_i n_k A_{kj}. \tag{5}$$

The symmetric strain-rate tensor A_{ij} and the vector $\mathbf{N}$, which gives the rate of change of the director relative to the fluid, are

$$A_{ij} = (\partial_i v_j + \partial_j v_i)/2,$$

$$\mathbf{N} = (\partial_t + \mathbf{v}\cdot\boldsymbol{\nabla})\mathbf{n} - \boldsymbol{\omega}\times\mathbf{n}. \tag{6}$$

Here $\boldsymbol{\omega} = (\boldsymbol{\nabla}\times\mathbf{v})/2$ is the local fluid rotation. The Leslie coefficients satisfy the Parodi relation $\alpha_2 + \alpha_3 = \alpha_6 - \alpha_5$ [19]. In addition, we assume incompressibility of the fluid (the density ρ_m is constant),

$$\boldsymbol{\nabla}\cdot\mathbf{v} = 0. \tag{7}$$

The equation for the director $\mathbf{n}$ is

$$\gamma_1(\partial_t + \mathbf{v}\cdot\boldsymbol{\nabla} - \boldsymbol{\omega}\times)\mathbf{n} = -\underline{\underline{\delta}}^{\perp}(\gamma_2\underline{\underline{A}}\mathbf{n} + \mathbf{h}), \tag{8}$$

where $\gamma_1 = \alpha_3 - \alpha_2$ is the rotational viscosity and $\gamma_2 = \alpha_3 + \alpha_2$. $\mathbf{h}$ is the molecular field obtained from the variational derivatives of the free-energy density F,

$$h_i = \frac{\delta F}{\delta n_i} = \frac{\partial F}{\partial n_i} - \partial_j\left(\frac{\partial F}{\partial n_{i,j}}\right), \quad i = x,y,z. \tag{9}$$

It should be noted that the variational derivatives are carried out at fixed electric field $\mathbf{E}$. The projection operator $\delta_{ij}^{\perp} = \delta_{ij} - n_i n_j$ in Eq. (8) ensures conservation of the normalization $\mathbf{n}^2 = 1$.

If the director $\mathbf{n}$ is driven by external forces (here by an optical field), then due to the coupling of Eqs. (1) and (8) a macroscopic flow can appear. Such a flow that appears as a result of director reorientation is called backflow.

B. Adiabatic elimination of the flow field

We will consider a nematic layer of thickness L situated in the $(\mathbf{x},\mathbf{y})$ plane. All physical quantities will be assumed to depend on (z,t) only. Then, from the incompressibility condition (7) and the no-slip boundary conditions

$$\mathbf{v}|_{z=0,L} = \mathbf{0} \tag{10}$$

one immediately concludes that the z component of the velocity vanishes,

$$\mathbf{v} = (v_x(z,t), v_y(z,t), 0), \tag{11}$$

so $\mathbf{v}$ is parallel to the plane of the layer. Moreover, all convective derivatives $\mathbf{v}\cdot\boldsymbol{\nabla}$ vanish.

We may distinguish two time scales in the hydrodynamic description: one is the director relaxation time τ, the other the momentum diffusion time τ_{visc} which is associated with the relaxation of $\mathbf{v}$ (actually with the vorticity of $\mathbf{v}$),

$$\tau = \frac{\gamma_1 L^2}{\pi^2 K_3}, \quad \tau_{visc} = \frac{\rho_m L^2}{\gamma_1}. \tag{12}$$

Typically $\tau \sim 1$ s and $\tau_{visc} \sim 10^{-6}$ s. Using the fact that $\tau_{visc} \ll \tau$, the Navier-Stokes equation (1) can be considerably simplified as the velocity follows adiabatically the motion of the director. Thus, the whole left-hand side of Eq. (1) can be neglected. In the absence of x, y dependence, the only contributions to Eq. (1) come from $j=z$. Finally, taking into account that $\pi_{xz}=\pi_{yz}=0$ since $\partial_x n_k = \partial_y n_k = 0$ [see Eq. (2)], the following relations are obtained from Eq. (1):

$$-T^{visc}_{xz}(z,t) = C_x(t),$$

$$-T^{visc}_{yz}(z,t) = C_y(t), \tag{13}$$

where $C_x(t)$ and $C_y(t)$ are functions that do not depend on z and will be fixed by the boundary conditions. The third equation following from Eq. (1) can be used to find the pressure $p(z,t)$ but this is not of interest here. Straightforward calculations of T^{visc}_{xz} from Eqs. (5) lead to

$$-T^{visc}_{xz}(z,t) = \left(\alpha_2 n_z - \alpha_3 \frac{n_x^2}{n_z}\right)\partial_t n_x - \alpha_3 \frac{n_x n_y}{n_z}\partial_t n_y + [2\alpha_1 n_x^2 n_z^2 + (\alpha_5 - \alpha_2) n_z^2 + (\alpha_3 + \alpha_6) n_x^2 + \alpha_4]\frac{U}{2} + n_x n_y [2\alpha_1 n_z^2 + \alpha_3 + \alpha_6]\frac{V}{2} = C_x(t), \tag{14}$$

where $U=\partial_z v_x$ and $V=\partial_z v_y$. The equation for T^{visc}_{yz} is obtained from Eq. (14) by interchanging the indices x and y (note that U and V are also interchanged).

The director equations (8) reduced to

$$\gamma_1 \partial_t n_x + n_z[(\alpha_2 - \gamma_2 n_x^2)U - \gamma_2 n_x n_y V] = \mathcal{L}_x, \tag{15}$$

$$\gamma_1 \partial_t n_y + n_z[(\alpha_2 - \gamma_2 n_y^2)V - \gamma_2 n_x n_y U] = \mathcal{L}_y, \tag{16}$$

where

$$\mathcal{L}_i = -[\underline{\delta}^{\perp}\mathbf{h}]_i, \quad i = x,y \tag{17}$$

is the corresponding component of the sum of the elastic and external (in our case optical) torques acting on the director. The expressions will be given later.

As a next step, we use Eqs. (15) and (16) to eliminate the time derivatives of the director from Eq. (14). The procedure is analogous to that used in [20] for a simpler situation. We are left with the following equations for the velocity gradients U, V:

$$\begin{pmatrix} g_x & a \\ a & g_y \end{pmatrix}\begin{pmatrix} U \\ V \end{pmatrix} + \begin{pmatrix} f_x \\ f_y \end{pmatrix} = \begin{pmatrix} C_x \\ C_y \end{pmatrix}, \tag{18}$$

where

$$a = \frac{n_x n_y}{2\gamma_1}[\gamma_2(\alpha_2 + 2\alpha_3) + \gamma_1(\alpha_5 + 2\alpha_1) - 2(\gamma_2^2 + \alpha_1\gamma_1)(n_x^2 + n_y^2)],$$

$$g_x = a\frac{n_x}{n_y} - \frac{1}{2\gamma_1}\{[\gamma_1(\alpha_2 - \alpha_5) + 2\alpha_2^2]n_z^2 - \alpha_4\gamma_1\},$$

$$f_x = \frac{1}{\gamma_1 n_z}[(\alpha_2 n_z^2 - \alpha_3 n_x^2)\mathcal{L}_x - \alpha_3 n_x n_y \mathcal{L}_y]. \tag{19}$$

g_y and f_y are obtained by interchanging the indices x and y in the expressions for g_x and f_x. One can invert the matrix in Eqs. (18) and thus solve for U, V,

$$\begin{pmatrix} U \\ V \end{pmatrix} = \frac{1}{a^2 - g_x g_y}\begin{pmatrix} a(C_y - f_y) - g_y(C_x - f_x) \\ a(C_x - f_x) - g_x(C_y - f_y) \end{pmatrix}. \tag{20}$$

Equations (20) still contain the unknown quantities $C_x(t), C_y(t)$. They can be determined by integrating Eqs. (20) across the layer. The integrals of the left-hand side vanish due to the boundary conditions (10). Thus a set of linear equations for C_x and C_y is obtained that has the following solution:

$$C_x = \frac{I_1 I_{3y} + I_{3x} I_{2y}}{I_{2x} I_{2y} - I_1^2}, \quad C_y = \frac{I_1 I_{3x} + I_{3y} I_{2x}}{I_{2x} I_{2y} - I_1^2}, \tag{21}$$

where

$$I_1 = \int_0^L \frac{a}{a^2 - g_x g_y} dz, \quad I_{2x} = \int_0^L \frac{g_y}{a^2 - g_x g_y} dz,$$

$$I_{3x} = \int_0^L \frac{g_y f_x - a f_y}{a^2 - g_x g_y} dz. \tag{22}$$

I_{2y} and I_{3y} are obtained by interchanging the indices x and y in the expressions for I_{2x} and I_{3x}, respectively.

Thus, by using Eqs. (20)–(22), the velocity gradients U, V can be eliminated from the director Eqs. (15) and (16).

C. The angle representation

From here on we will use normalized time $t \to t/\tau$, length $z \to \pi z/L$, and viscosity coefficients $\alpha_i \to \alpha_i/\gamma_1$ (the same symbols will be kept). We will also introduce dimensionless elasticities $k_1 = K_1/K_3$, $k_2 = K_2/K_3$.

Next we introduce the representation adapted to our geometry in terms of the spherical angles $\Theta(z,t)$ and $\Phi(z,t)$ such that (see Fig. 1)

$$\mathbf{n} = (\sin\Theta\cos\Phi, \sin\Theta\sin\Phi, \cos\Theta). \tag{23}$$

We write

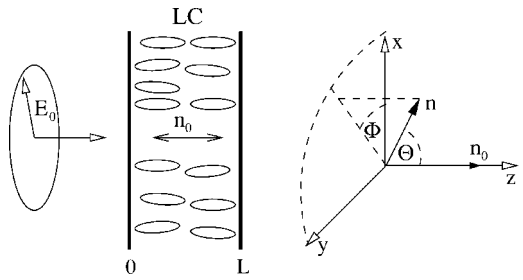

FIG. 1. Geometry of the setup: circularly polarized light incident perpendicularly on a nematic layer with the director $\mathbf{n}_0 \| \mathbf{z}$ (homeotropic state). The components of the director $\mathbf{n}$ are described in terms of the angles Θ, Φ ($\Theta = 0$ in the homeotropic state).

$$\Phi = \Phi_0(t) + \Phi_d(z,t), \tag{24}$$

where $\Phi_0(t)$ does not depend on z and describes a rigid rotation of the director around the z axis (no distortion) while $\Phi_d(z,t)$ includes twist distortion. The decomposition (24) is not unique in the sense that any constant can be added to Φ_0 and then subtracted from Φ_d. The key point, however, is that Φ_0 depends on time only and can be unbounded while Φ_d is required to remain bounded.

To derive the equation of motion for Θ and Φ, we substitute the expression for the director (23) into Eqs. (15) and (16) and use Eqs. (20)–(22) for the velocity elimination. We arrive at

$$\partial_t \Theta = \left[1 + \frac{2\mu^2}{g_{11}+g_{12}}\right]\mathcal{L}_\Theta - \frac{4\mu}{g_{11}+g_{12}}(D_1 \cos\Phi_d + D_2 \sin\Phi_d), \tag{25}$$

$$\partial_t \Phi = \left[1 + \frac{2\alpha_2^2 \cos^2\Theta}{g_{11}}\right]\mathcal{L}_\Phi + \frac{4\alpha_2 \cot\Theta}{g_{11}}(D_1 \sin\Phi_d - D_2 \cos\Phi_d), \tag{26}$$

where the unknown quantities $D_1(t), D_2(t)$ as well as μ, g_{11}, and g_{12} are given in Appendix A, Eqs. (A1)–(A3). $\mathcal{L}_\Theta$ and $\mathcal{L}_\Phi$ are the torques in the angle representation. We decompose the torques into their elastic and external parts,

$$\mathcal{L}_\Theta = \mathcal{L}_\Theta^{(elast)} + \mathcal{L}_\Theta^{(ext)}, \quad \mathcal{L}_\Phi = \mathcal{L}_\Phi^{(elast)} + \mathcal{L}_\Phi^{(ext)}. \tag{27}$$

Calculating the elastic contributions explicitly from Eqs. (3), (9), and (17), we find

$$\mathcal{L}_\Theta^{(elast)} = [1 - (1-k_1)\sin^2\Theta]\partial_z^2\Theta - \frac{\sin 2\Theta}{2}\{(1-k_1)(\partial_z\Theta)^2 + [1 - 2(1-k_2)\sin^2\Theta](\partial_z\Phi)^2\},$$

$$\mathcal{L}_\Phi^{(elast)} = \frac{1}{\sin^2\Theta}\frac{\partial}{\partial z}\{[1-(1-k_2)\sin^2\Theta]\sin^2\Theta\partial_z\Phi\}. \tag{28}$$

Transforming external contributions from Cartesian to spherical coordinates, we obtain

$$\mathcal{L}_\Theta^{(ext)} = \left(\frac{L}{\pi}\right)^2 \frac{1}{K_3}(\mathcal{L}_x^{(ext)} \cos\Phi + \mathcal{L}_y^{(ext)} \sin\Phi),$$

$$\mathcal{L}_\Phi^{(ext)} = \left(\frac{L}{\pi}\right)^2 \frac{1}{K_3}(\mathcal{L}_y^{(ext)} \cos\Phi - \mathcal{L}_x^{(ext)} \sin\Phi). \tag{29}$$

The prefactor in the external torques results from the normalization.

Note that the external torque acting on the director is still not specified, i.e., the derived director equations can be applied to other problems.

The boundary conditions on Θ and Φ are (strong homeotropic anchoring)

$$\Theta|_{z=0,\pi} = 0, \quad \partial_z\Phi|_{z=0,\pi} = 0. \tag{30}$$

It should be noted that sometimes (for simplicity), instead of Eq. (10), the following unrealistic boundary conditions are used for the velocity field [21]:

$$U|_{z=0,L} = V|_{z=0,L} = 0 \tag{31}$$

(stress-free boundaries). One can immediately conclude in this case from Eqs. (13) that $T_{xz}^{visc}|_{z=0,L} = T_{yz}^{visc}|_{z=0,L} = 0$, which gives $C_x = C_y = 0$ as well as $D_1 = D_2 = 0$. Finally, the director equations (15) and (16) or (25) and (26) are considerably simplified and the backflow effect manifests itself just in a renormalization of the viscosity γ_1. However, such boundary conditions cannot be realized in a real experiment.

D. The optical torque

We will consider a circularly polarized plane wave incident perpendicularly on the nematic layer. The light is polarized in the plane of the layer [the $(\mathbf{x},\mathbf{y})$ plane] and propagates along the positive $\mathbf{z}$ axis (see Fig. 1). We consider the case where the diameter of the laser beam is much larger than the thickness of the layer. Thus we can assume that all quantities depend only on z,t. Then the light inside the nematic is treated as a plane wave.

We calculate the optical torque from Eqs. (4), (9), and (17). The electric fields obtained from Maxwell's equations are written in terms of the amplitudes of the ordinary and the extraordinary waves A_o, A_e, and the phase delay between these two waves induced by the nematic slice $\alpha(z)$, see Eqs. (B11). A_o, A_e, and $\alpha(z)$ are determined from Eqs. (B6)–(B10). One finally finds

$$\mathcal{L}_\Theta^{(ext)} = \rho \sin 2\Theta \left(\frac{\lambda_e}{\lambda_o}\right)^2 |A_e|^2,$$

$$\mathcal{L}_\Phi^{(ext)} = 2\rho\frac{\lambda_e}{\lambda_o}\,\mathrm{Re}[A_e A_o^\star \mathbf{e}^{i\alpha(z)}]. \tag{32}$$

Here λ_o, λ_e are the squares of the indices of refraction for the ordinary and extraordinary waves given by Eq. (B8). In Eqs. (32), $\rho = I/I_c$ is the dimensionless incident light intensity, with the LIFT threshold intensity given by

$$I_c = \frac{2\pi^2}{L^2}\frac{c(\varepsilon_\perp + \varepsilon_a)K_3}{\varepsilon_a\sqrt{\varepsilon_\perp}}, \tag{33}$$

where c is the velocity of light in vacuum. The expression (33) will be verified in the next section by showing that $\rho = 1$ indeed corresponds to the linear threshold.

Thus, we have to solve the director equations (25) and (26) with boundary conditions (30) coupled with the ODEs for the amplitudes of the electric field (B6) with initial conditions (B10). Because of isotropy in the (x,y) plane, the equations are invariant under a rotation around the z axis ($\Phi \to \Phi + \delta\Phi$). This can be seen from the fact that the torques given in Eqs. (28) and (32) do not depend on Φ (only on $\partial_z\Phi$).

III. LINEAR STABILITY ANALYSIS OF THE BASIC STATE

We performed a linear stability analysis around the homeotropic state $\Theta = 0$ with Φ undefined. When the light propagates through the LC with homeotropic orientation, its polarization remains unchanged and the phase delay $\alpha(z)$ is zero. We linearize Eq. (25) in Θ. The linear part of $\mathcal{L}_\Theta$ is

$$\mathcal{L}_\Theta = \partial_z^2\Theta + 2\rho\Theta|A_{e0}|^2 = \partial_z^2\Theta + \rho\Theta \tag{34}$$

[see Eq. (B10)]. Linearization of the terms proportional to D_1, D_2 leads to the formula

$$D_1 \cos\Phi_d + D_2 \sin\Phi_d = -\frac{I_2}{I_5}, \tag{35}$$

where I_2 and I_5 are the integrals defined in Eq. (A2). In this approximation, they are given by

$$I_2 = -\frac{b}{2\alpha_2(1-b)}\int_0^\pi \mathcal{L}_\Theta dz, \quad I_5 = \frac{\pi b}{\alpha_2^2(1-b)} \tag{36}$$

with

$$b = \frac{2\alpha_2^2}{\alpha_4 + \alpha_5 - \alpha_2} = \frac{\alpha_2^2}{\eta_2} > 0, \tag{37}$$

where $\eta_2 = (\alpha_4 + \alpha_5 - \alpha_2)/2$ is an effective viscosity [11]. Finally, the linearized equation (25) has the form

$$(1-b)\partial_t(\Theta) = \mathcal{L}_\Theta - \frac{b}{\pi}\int_0^\pi \mathcal{L}_\Theta dz. \tag{38}$$

We look for solutions of the form

$$\Theta(z,t) = \Theta(z)e^{\sigma t}, \tag{39}$$

where σ is the growth rate and we obtain from Eqs. (34) and (38)

$$\partial_z^2\Theta + [\rho - \sigma(1-b)]\Theta - \frac{b}{\pi}\int_0^\pi dz[\partial_z^2\Theta + \rho\Theta] = 0. \tag{40}$$

Taking into account the boundary conditions $\Theta|_{z=0,\pi} = 0$, Eq. (40) is solved by

TABLE I. Viscosity coefficients for the nematic 5CB at $T = 26\ ^\circ$C (see Ahlers in [22]). $\alpha_6 = \alpha_2 + \alpha_3 + \alpha_5$ (Parodi relation).

Viscosities	α_1	α_2	α_3	α_4	α_5
In units of dyn s/cm^2	−0.066	−0.77	−0.042	0.634	0.624
Normalized to γ_1	−0.091	−1.058	−0.058	0.871	0.857

$$\Theta = -\cos\left[\frac{\pi}{2}\delta\right] + \cos\left[\left(\frac{\pi}{2} - z\right)\delta\right], \tag{41}$$

where $\delta(\rho)$ satisfies the transcendental equation

$$2b(\delta^2 - \rho)\sin\left[\frac{\pi}{2}\delta\right] + \delta(b\rho - \delta^2)\pi\cos\left[\frac{\pi}{2}\delta\right] = 0 \tag{42}$$

and

$$\sigma = \frac{\rho - \delta^2}{1-b}. \tag{43}$$

Noting that $\rho = \delta = 1$ is a solution of Eq. (42), we expand the equation with respect to δ and ρ around this point. To lowest order, one finds

$$\delta = 1 + \frac{4b(\rho - 1)}{\pi^2(1-b) + 8b}. \tag{44}$$

Finally, the growth rate $\tilde{\sigma} = \sigma/\tau$ in physical units can be written as

$$\tilde{\sigma} = \frac{\rho - 1}{\tau\xi}, \tag{45}$$

where

$$\xi = 1 - \left(1 - \frac{8}{\pi^2}\right)b = 1 - 0.19\frac{\alpha_2^2}{\eta_2}. \tag{46}$$

One can see from Eq. (45) that the homeotropic state loses stability at $\rho = 1$. Replacing ξ by 1 corresponds to the neglect of backflow. Thus, within the linear approximation, backflow results in a renormalization of the rotational viscosity γ_1 (in fact a reduction). The same expression for the reduction factor ξ was found in [12] where a one-mode approximation for the director components and smallness of the twist distortion were used. Our derivation is exact within the linearization around the homeotropic state.

In the calculations, we took the viscosity coefficients for the nematic 5CB (see Table I). For these parameters, the value of ξ turns out to be $\xi \simeq 0.85$. For (unrealistic) stress-free boundary conditions [see Eq. (31)], one obtains $\xi = 1 - b \simeq 0.20$.

IV. SIMULATIONS

As a next step, we simulated the dynamic equations listed at the end of Sec. II. For this purpose, we expand Θ and Φ with respect to z in systems of orthogonal functions which satisfy the boundary conditions (30),

$$\Theta = \sum_{n=1}^{\infty} \Theta_n(t) V_n(z),$$

$$\Phi \equiv \Phi_0(t) + \Phi_d(z,t) = \Phi_0(t) + \sum_{n=1}^{\infty} \Phi_n(t) U_n(z), \quad (47)$$

where $V_n(z)$ are harmonic functions and $U_n(z)$ are the Chebyshev polynomials of the second kind [23],

$$V_n(z) = \sin nz, \quad U_n(z) = \frac{\sin(n+1)z}{\sin z}, \quad (48)$$

which are normalized as

$$\int_0^{\pi} dz V_m(z) V_n(z) = \int_0^{\pi} dz U_m(z) U_n(z) \sin^2 z = \frac{\pi}{2} \delta_{mn}. \quad (49)$$

After substituting the expansions (47) into Eqs. (25) and (26) and projecting Eq. (25) onto the modes Θ_n and Eq. (26) onto Φ_n (Galerkin method), a set of coupled nonlinear ODEs for the modes $\Theta_n(t)$, $\Phi_n(t)$ is obtained,

$$\frac{d\Phi_n}{dt} = \mathcal{G}_n(\Theta_1, \Theta_2, \ldots; \Phi_1, \Phi_2, \ldots),$$

$$\frac{d\Theta_n}{dt} = \mathcal{F}_n(\Theta_1, \Theta_2, \ldots; \Phi_1, \Phi_2, \ldots), \quad n = 1,2, \ldots . \quad (50)$$

The infinite set of ODEs given by Eqs. (50) was truncated and solved by a standard Runge-Kutta method. The number of modes was chosen such that the estimated accuracy of the calculated director components was better than 1% (we took ten modes on both angles). The ODEs for A_o, A_e [Eq. (B6)] were solved at each time step. Note that neither Eq. (50) nor Eq. (B6) with initial conditions (B10) contains the zeroth mode Φ_0. Thus, the ODE for $\Phi_0(t)$ does not couple back to Eqs. (50) (as a result of isotropy),

$$\frac{d\Phi_0}{dt} = \mathcal{G}_0(\Theta_1, \Theta_2, \ldots; \Phi_1, \Phi_2, \ldots). \quad (51)$$

The procedure becomes more complicated compared to the case without backflow because of the appearance of the integrals (A2) that have to be evaluated at each time step.

When Θ_n and Φ_n do not depend on t [$d\Phi_n/dt = d\Theta_n/dt = 0$], the angular velocity $d\Phi_0/dt$ is a constant and the director precesses uniformly around the z axis with a frequency

$$f_0 = \frac{1}{2\pi} \frac{d\Phi_0}{dt}. \quad (52)$$

In this case, the problem is significantly simplified. In fact, instead of solving a system of evolution equations for $\Phi_n(t)$ and $\Theta_n(t)$, we are now faced with a set of nonlinear algebraic equations. After solving them by a Newton-Raphson method and substituting Φ_n and Θ_n into Eq. (51), the frequency f_0 of the uniform precession can be found. We call such a state a uniform precession (UP) state. Furthermore, the linear stability analysis of a UP state can be performed by calculating the eigenvalues of the Jacobian matrix $J_{ij} = (\partial F_i / \partial \mathbf{x}_j)_{\mathbf{x}=\mathbf{x}_{\mathrm{UP}}}$, where

$$\mathbf{x} = (\Theta_1, \ldots, \Theta_N, \Phi_1, \ldots, \Phi_M)$$

and

$$\mathbf{F} = (\mathcal{G}_1, \ldots, \mathcal{G}_n; \mathcal{F}_1, \ldots, \mathcal{F}_n).$$

The preceding discussion holds only for circularly polarized light since for elliptical polarization the rotational invariance is broken. This considerably enriches the dynamics [24–26].

In the calculations, we used the known material parameters for the nematic E7, as in [8,9] (where the backflow was not included): $K_1 = 11.09 \times 10^{-7}$ dyn, $K_2 = 5.82 \times 10^{-7}$ dyn, $K_3 = 15.97 \times 10^{-7}$ dyn [25], $n_e = 1.746$, $n_o = 1.522$ [27] (refractive indices of the ordinary and extraordinary light, respectively). The viscosities, which are not known for E7, were taken from 5CB, see Table I. The calculations were made for a laser wavelength of $\lambda = 532$ nm and a layer thickness of 100 μm. For these parameters $I_c \simeq 2.6$ kW/cm^2, $\tau \simeq 4.6$ s.

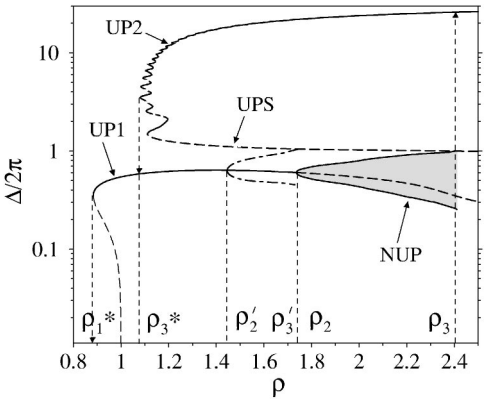

FIG. 2. $\Delta/2\pi$ versus ρ in semilogarithmic scale. Solid (dashed) curves correspond to stable (unstable) UP solutions. Gray region: nonuniform precession states of the director. Dash-dotted lines in the (ρ_2', ρ_3') interval: nonuniform precession states of the director when backflow is neglected. The fact that $\rho_3' \simeq \rho_2$ is accidental.

V. BIFURCATION SCENARIO

This section gives an overview of the bifurcation scenario occurring in the system. It turns out that the qualitative features are not changed by the backflow (see [8,9] for details).

We will use the phase delay $\Delta \equiv \alpha(z=\pi)$ between the ordinary and the extraordinary wave induced by the whole layer, see Eq. (B9), to characterize the output state. Δ depends on Θ only and is a global measure of the amplitude of reorientation. It has a direct experimental interpretation since the quantity $\Delta/2\pi$ represents roughly the number of self-diffraction rings in the far field [28].

In Fig. 2, $\Delta/2\pi$ is plotted versus the normalized intensity ρ. The solid lines represent stable uniform precession (UP) states, while the dashed lines correspond to precession states that are unstable. The region in gray corresponds to a non-

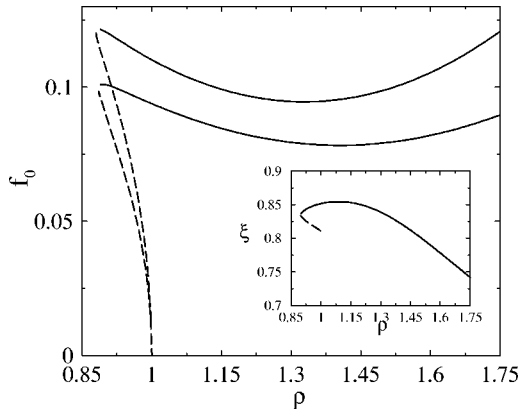

FIG. 3. Dimensionless precession frequency f_0 versus ρ for the case with (upper line) and without backflow. Solid (dashed) curves correspond to stable (unstable) solutions. Inset: $\xi=f_0^\star/f_0$ versus ρ, where f_0 ($f_0^\star$) is the precession frequency when the backflow is (not) included.

uniform precession (NUP) where nutation ($d\Delta/dt\neq 0$) is coupled to precession. In this regime, the lower and the upper lines that limit the region correspond to the minimum and maximum values taken by Δ during its oscillation. The UP lines are practically unchanged by the backflow. The NUP region without backflow extends from ρ_2' to ρ_3' (included in Fig. 2).

The optical Fréedericksz transition occurs at $\rho=1$ via a subcritical Hopf-type bifurcation where the system settles to a uniform precession state with a small reorientation amplitude ($\Delta\sim\pi$ so that $\Theta^2\ll 1$, since $L/\lambda\gg 1$ [5]) labeled UP1. Decreasing the intensity from the UP1 regime, the system switches back to the unperturbed state at $\rho=\rho_1^*\simeq 0.88$ where a saddle-node bifurcation occurs. The trajectory in the (n_x,n_y) plane is a circle, whereas in a coordinate system that rotates with frequency f_0 around the z axis it is a fixed point. The time Fourier spectra of the director $\mathbf{n}$ and velocity $\mathbf{v}$ have one fundamental frequency f_0. Θ_n, Φ_n, and Δ do not depend on time.

In Fig. 3, the precession frequency f_0 of the UP1 state versus ρ is shown for the case with and without backflow. As expected, the backflow results in an increase of f_0 because γ_1 effectively decreases. The ratio $\xi=f_0^\star/f_0<1$, where f_0 ($f_0^\star$) is the precession frequency when the backflow is (is not) included, is shown by the inset in Fig. 3. It turns out that ξ has a maximum near $\rho=1.1$. The maximal value is near to the damping factor $\xi\simeq 0.85$ obtained from the linear stability analysis of the homeotropic state (see Sec. III), but for larger intensities it decreases substantially.

With further increase of the intensity, the UP1 loses stability via a supercritical Hopf bifurcation at $\rho=\rho_2$ where the director starts to nutate (NUP regime). For the NUP state, all modes Θ_n and Φ_n with $n\geqslant 1$ are time-dependent and their Fourier spectrum contains frequencies mf_1, where m is an integer. The spectra of the phase delay Δ, director $\mathbf{n}$, and velocity $\mathbf{v}$ have contributions at frequencies given by the simple formulas

$$\tilde{\Delta}=\{mf_1\},$$

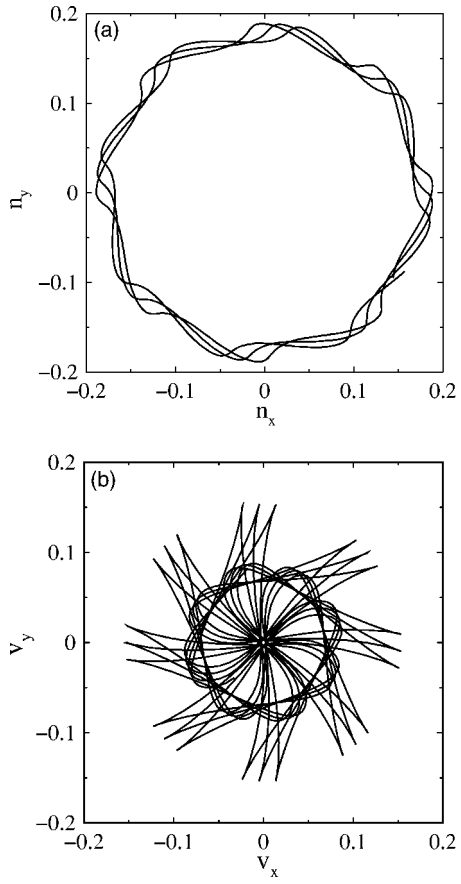

FIG. 4. Typical phase portraits in the (n_x,n_y) (a) and (v_x,v_y) (b) plane for the NUP regime ($\rho=1.80$) at some fixed value of z. The trajectories are plotted for the same time interval in both cases. v_x,v_y are dimensionless.

$$\tilde{\mathbf{n}}=\{f_0,mf_1\pm f_0\},$$

$$\tilde{\mathbf{v}}=\{f_0,mf_1\pm 2f_0\}. \tag{53}$$

In Figs. 4(a) and 4(b), a typical trajectory in the (n_x,n_y) and (v_x,v_y) plane is shown at $z=\pi/2-\ell$ ($\ell=0.1$) for the NUP state. The reason for this somewhat arbitrary value of z is to have contributions from all polar modes since for the even n, $\Theta_n\sin(nz)$ is zero at the center of the cell ($z=\pi/2$). The trajectories in the laboratory frame (shown) are not closed because the director (as the flow) is characterized by two incommensurate frequencies f_0 (precession) and f_1 (nutation). However, the director (as the flow) performs a simple periodic motion with a frequency f_1 in the frame that rotates with frequency f_0 around the z axis. It should be pointed out that the time averages of v_x and v_y are zero (no external flow).

In some narrow region around $\rho_3\approx 2.4$, the period $T=1/f_1$ of the NUP increases progressively with increasing light intensity, and indeed appears to diverge logarithmically at ρ_3. Thus as ρ approaches ρ_3, the NUP limit cycle collides with the unstable UPS branch represented by a saddle. In fact, we deal here with *a homoclinic bifurcation* of the simplest type where a limit cycle collides with a saddle point

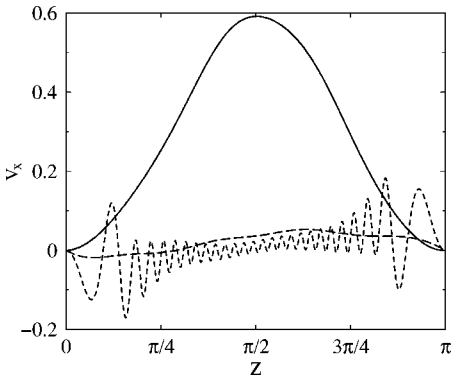

FIG. 5. Profiles of the dimensionless v_x versus normalized z at times when the respective spatial maximum is maximal. Long-dashed line: UP1 state ($\rho=1.70$). Solid line: NUP state rather close to the homoclinic bifurcation ($\rho=2.30$) where one has pronounced maxima in time. Dashed line: UP2 state ($\rho=2.30$). The dimensionless velocity $v_x \simeq 0.6$ corresponds to 4 μm/s.

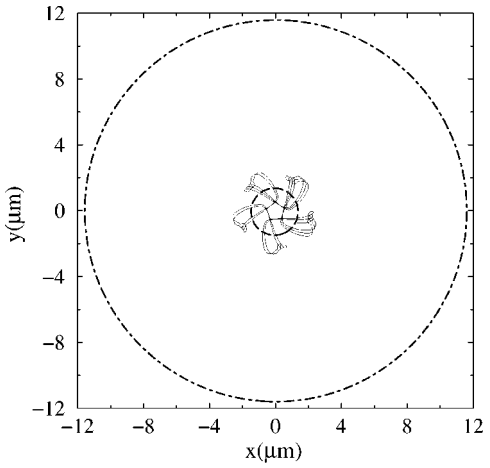

FIG. 6. Trajectories of the fluid motion for different states of the director motion. Long-dashed curve: UP1 state ($\rho=1.70$). Solid line: NUP state ($\rho=2.30$). Dot-dashed line: UP2 state ($\rho=2.30$).

having only one unstable direction [29] (all the eigenvalues have negative real parts except one, which is real and positive).

At $\rho=\rho_3$, the system switches abruptly to a uniform precession with large reorientation amplitude ($\Theta^2 \sim 1$ so that $\Delta \gg 1$) labeled UP2. Note that the period of precession $1/f_0$ is several orders of magnitude larger than that in the UP1 and NUP regimes. Decreasing the intensity in the UP2 regime, the system switches back to the UP1 regime at $\rho=\rho_3^* \simeq 1.08$. It is worth noting that the unstable UP1 branch ($\rho > \rho_2$) makes a loop (not shown in Fig. 2) and connects with the other unstable uniform precession branch, UPS, which itself connects with UP2 (see Fig. 2).

The phase delay Δ for the UP regimes is only slightly different from the case without backflow. However, the regime of nonuniform director precession (NUP) shifts to higher intensities. As is seen from Fig. 2, the thresholds for the NUP and for the UP2 regimes turn out to be $\rho_2=1.75$ and $\rho_3=2.4$ instead of $\rho_2'=1.45$ and $\rho_3'=1.75$ when the backflow is neglected [8,9]. Thus the backflow leads to a quantitative change of the bifurcation scenario.

In Fig. 5, typical profiles for the velocity component v_x versus z (at a fixed time t where v_x has maximal amplitude) are shown for a UP1, UP2, and NUP state. One can see that the amplitude of the velocity in the NUP regime is significantly larger than that for the UP regimes. An interesting and, at first sight, surprising fact is that for the UP2 state, v_x oscillates fairly rapidly across the cell. The reason is that the interference structure of the ordinary and the extraordinary light for the UP2 states leads to an oscillating behavior of the electric part of the torque [see the expression for $\mathcal{L}_\Phi$ in Eq. (32)] resulting in a similar structure in $\partial_z \Phi_d$, which drives the velocity field. This occurs only for $\Delta=\alpha(\pi) \gg 1$, as is the case for the UP2 states. For $\rho=2.3$, one has $\Delta/2\pi \simeq 25.5$, see Fig. 2, and there are indeed 26 minima in the velocity field of Fig. 5. Since in the UP1 and NUP regimes Δ is always less than 2π, the velocity field has only one or two extrema.

In Fig. 6, the typical trajectories of the fluid motion occurring in the (x,y) plane for the UP1, NUP, and UP2 states are shown at a fixed value of $z=\pi/2-0.1$, where $x(t) = \int_0^t v_x(t')dt'$ and $y(t)=\int_0^t v_y(t')dt'$. The period of the fluid motion is characterized by the period of precession $T_0 = 1/f_0$ for UP states and by both T_0 and the period of nutation $T_1=1/f_1$ for the NUP state. In present example, T_0 turns out to be $T_0 \simeq 9\tau$ and $T_0 \simeq 147\tau$ for the UP1 state ($\rho=1.70$) and for the UP2 state ($\rho=2.30$) respectively. For the NUP state ($\rho=2.30$), we found $T_0 \simeq 10\tau$ and $T_1 \simeq 2\tau$. One can conclude that the fluid motion differs qualitatively for three types of states. Indeed, for the UP2 state, the fluid motion develops along a circle with the radius that is much larger than that for the UP1 state. Furthermore, in the latter case the motion is much faster. It is also qualitatively different from that for the NUP state, as is seen from Fig. 6. We thus speculate that the backflow can act as a sensitive diagnostic to distinguish the three types of director motion.

VI. CONCLUSION

In the present article, we have examined the influence of backflow on the director dynamics when driven by circularly polarized light. For this purpose we have, after adiabatic elimination of the flow field, performed a linear stability analysis around the basic state in order to assess the "linearized viscosity reduction factor." Then we have simulated the full set of nematodynamic equations and demonstrated that backflow does not lead to qualitative changes in the dynamical scenario, but does lead to substantial quantitative changes in the secondary bifurcation thresholds. It turns out that the regime of nonuniform precession shifts to higher light intensities by about 20% and exists in a larger interval. However, the experimental values of the thresholds ρ_2, ρ_3 are even smaller than that given by the theory without backflow [9]. One is now forced to conclude that the discrepancy between the theoretical predictions and the experiment is strongly affected by the fact that in the experiments the beam size was not large compared to the layer thickness, as assumed in our theory. In fact, the beam size was of the order of the layer thickness. By using a large aspect-ratio geometry, one is now (after this calculation) in a position to test the theoretical

framework quantitatively. This can be done by use of the dye-doped nematic because the values of LIFT in this case can be two orders of magnitude smaller than for a pure nematic (see [30,31] and references therein). The fact that the threshold intensity is low allows the spot size of the light to be much larger than the thickness of the layer, thus the plane-wave approximation assumed in the theory might be better achieved in the experiment.

We have also found an unanticipated spatial oscillation of the backflow in the UP2 regime. It results from spatial oscillations of the director twist $\partial_z\Phi$, which are a consequence of oscillations in the torque resulting from interference phenomena between ordinary and extraordinary light. Possibly the strong differences of the flow in the various states can be observed by visualizing the flow field using small dissolved tracer particles, see, e.g., [32]. In that case, we expect that the circular trajectories [in the (x,y) plane] with different rotation sign (and radius amplitude) for particles lying in different z positions will be especially visible for UP2 states signifying the spatial oscillation across z.

ACKNOWLEDGMENTS

We wish to thank E. Brasselet for useful discussions. Financial support by the Deutsche Forschungsgemeinschaft under Kr 690/16, 436UNG113/151/1, and Kr 690/22 is gratefully acknowledged.

APPENDIX A: THE EXPRESSIONS FOR D_1, D_2

Straightforward calculations give the following expressions for D_1, D_2 needed in Eqs. (25) and (26):

$$D_1 = \frac{I_2(I_4 - I_5) + I_1 I_3}{I_5^2 - I_3^2 - I_4^2}, \quad D_2 = \frac{I_1(I_4 + I_5) - I_2 I_3}{I_5^2 - I_3^2 - I_4^2}, \quad \text{(A1)}$$

with

$$I_1 = \int_0^\pi \left\{ \frac{\alpha_2 \sin 2\Theta \mathcal{L}_\Phi \cos \Phi_d}{2g_{11}} + \frac{\mu \mathcal{L}_\Theta \sin \Phi_d}{g_{11} + g_{12}} \right\} dz,$$

$$I_2 = \int_0^\pi \left\{ \frac{\alpha_2 \sin 2\Theta \mathcal{L}_\Phi \sin \Phi_d}{2g_{11}} - \frac{\mu \mathcal{L}_\Theta \cos \Phi_d}{g_{11} + g_{12}} \right\} dz,$$

$$I_3 = \int_0^\pi \frac{g_{12} \sin 2\Phi_d}{g_{11}(g_{11} + g_{12})} dz,$$

$$I_4 = -\int_0^\pi \frac{g_{12} \cos 2\Phi_d}{g_{11}(g_{11} + g_{12})} dz,$$

$$I_5 = \int_0^\pi \frac{2g_{11} + g_{12}}{g_{11}(g_{11} + g_{12})} dz. \quad \text{(A2)}$$

Here μ, g_{11}, and g_{12} depend on Θ only,

$$\mu(\Theta) = \alpha_2 - \gamma_2 \sin^2 \Theta,$$

$$g_{11}(\Theta) = \alpha_4 + [\alpha_5 - \alpha_2 - 2\alpha_2^2] \cos^2 \Theta,$$

$$g_{12}(\Theta) = (\alpha_5 - \alpha_2 \gamma_2 + 2[\alpha_1 + \gamma_2^2] \cos^2 \Theta) \sin^2 \Theta. \quad \text{(A3)}$$

APPENDIX B: EQUATIONS FOR THE LIGHT PROPAGATION

Maxwell's equations contain the dielectric tensor that depends on the director components

$$\varepsilon_{ij} = \varepsilon_\perp \delta_{ij} + \varepsilon_a n_i n_j, \quad \text{(B1)}$$

where $\varepsilon_a = \varepsilon_\parallel - \varepsilon_\perp$ is the dielectric anisotropy and $\varepsilon_\perp$ ($\varepsilon_\parallel$) is the dielectric permittivity perpendicular (parallel) to **n**. We write the electric field in the form $\mathbf{E}(\mathbf{r},t) = 1/2[\mathbf{E}(z,t)e^{-i\omega t} + \text{c.c.}]$, where $k_0 = \omega/c$ is the wave number in vacuum and $\mathbf{E}(z,t)$ is the amplitude that varies slowly in time compared to ω^{-1} and obeys the equation

$$\frac{\partial^2}{\partial z^2} \begin{pmatrix} E_x \\ E_y \end{pmatrix} = -\frac{k_0^2}{\varepsilon_{zz}} \mathsf{M} \begin{pmatrix} E_x \\ E_y \end{pmatrix}, \quad \text{(B2)}$$

where

$$\mathsf{M} = \begin{pmatrix} \varepsilon_{xx}\varepsilon_{zz} - \varepsilon_{xz}^2 & \varepsilon_{xy}\varepsilon_{zz} - \varepsilon_{xz}\varepsilon_{yz} \\ \varepsilon_{xy}\varepsilon_{zz} - \varepsilon_{xz}\varepsilon_{yz} & \varepsilon_{yy}\varepsilon_{zz} - \varepsilon_{yz}^2 \end{pmatrix}$$

in case of perpendicular incidence. The z component of the electric field can be found from the following relation:

$$E_z = -\frac{\varepsilon_{xz}E_x + \varepsilon_{yz}E_y}{\varepsilon_{zz}}. \quad \text{(B3)}$$

We can now perform a transformation from the basis $(\mathbf{e}_x, \mathbf{e}_y)$ into the local basis $(\mathbf{e}_o, \mathbf{e}_e^\perp)$ where the matrix M has diagonal form [33]. In this new coordinate system, the field components are the amplitudes of the ordinary wave E_o and the transversal part of the extraordinary wave $E_e^\perp$ [note that $\mathbf{E}_e^\perp = \mathbf{E}_e - (\mathbf{E}_e \mathbf{e}_z)\mathbf{e}_z$] and are given by

$$\begin{pmatrix} E_o \\ E_e^\perp \end{pmatrix} = \begin{pmatrix} -\sin \Phi & \cos \Phi \\ \cos \Phi & \sin \Phi \end{pmatrix} \begin{pmatrix} E_x \\ E_y \end{pmatrix}. \quad \text{(B4)}$$

The transversal part of the electric field expressed in the two representations is

$$\mathbf{E}^\perp = E_x \mathbf{e}_x + E_y \mathbf{e}_y = E_e^\perp \mathbf{e}_e^\perp + E_o \mathbf{e}_o. \quad \text{(B5)}$$

Introducing dimensionless quantities $z \to z\pi/L$, $k_0 \to k_0 L/\pi$ (L is the thickness of the layer), and rewriting Eq. (B2) in terms of E_o, $E_{e\perp}$ under the *slowly varying envelope approximation* ($k_0 \gg 1$), the equations for the ordinary and extraordinary waves can be derived,

$$\partial_z A_o = -(\partial_z \Phi) \sqrt{\frac{\lambda_e}{\lambda_o}} \mathbf{e}^{i\alpha(z)} A_e,$$

$$\partial_z A_e = -\frac{(\partial_z \lambda_e) A_e}{4\lambda_e} + (\partial_z \Phi) \sqrt{\frac{\lambda_o}{\lambda_e}} \mathbf{e}^{-i\alpha(z)} A_o. \quad \text{(B6)}$$

A_o, A_e are amplitudes that vary slowly with z on the scale k_0^{-1} and are defined by

$$E_o = A_o \mathbf{e}^{ik_0\sqrt{\lambda_o}z}, \quad E_{e\perp} = A_e \mathbf{e}^{ik_0\int_0^z dz'\sqrt{\lambda_e(z')}} \tag{B7}$$

and

$$\lambda_o = \varepsilon_\perp, \quad \lambda_e = \frac{\varepsilon_\perp(\varepsilon_a + \varepsilon_\perp)}{\varepsilon_\perp + \varepsilon_a \cos^2\Theta}, \tag{B8}$$

$$\alpha(z) = k_0 \int_0^z (\sqrt{\lambda_e} - \sqrt{\lambda_o})dz. \tag{B9}$$

Here $\alpha(z)$ is the phase delay between the ordinary and extraordinary waves induced by the nematic slice of thickness z.

The initial conditions for the amplitudes A_o, A_e (normalized to the amplitude of the incoming light) at $z=0$ are

$$|A_{e0}|^2 = |A_{o0}|^2 = \frac{1}{2}, \quad A_{e0}A_{o0}^\star = \pm\frac{i}{2}, \tag{B10}$$

where the sign in Eq. (B10) defines the helicity of the incident light.

The components of the electric field E_x, E_y are related with A_e, A_o as follows:

$$|E_x|^2 = \cos^2\Phi|A_e|^2 - \sin 2\Phi\ \mathrm{Re}[A_e A_o^\star \mathbf{e}^{i\alpha(z)}] + \sin^2\Phi|A_o|^2,$$

$$|E_y|^2 = \cos^2\Phi|A_o|^2 + \sin 2\Phi\ \mathrm{Re}[A_e A_o^\star \mathbf{e}^{i\alpha(z)}] + \sin^2\Phi|A_e|^2,$$

$$E_x E_y^\star + E_x^\star E_y = \sin 2\Phi(|A_e|^2 - |A_o|^2) + 2\cos 2\Phi\ \mathrm{Re}[A_e A_o^\star \mathbf{e}^{-i\alpha(z)}]. \tag{B11}$$

[1] N. V. Tabiryan, A. V. Sukhov, and B. Y. Zel'dovich, Mol. Cryst. Liq. Cryst. **136**, 1 (1985).
[2] F. Simoni, *Nonlinear Optical Properties of Liquid Crystals* (World Scientific, Singapore, 1997).
[3] E. Santamato, B. Daino, M. Romagnoli, M. Settembre, and Y. R. Shen, Phys. Rev. Lett. **57**, 2423 (1986).
[4] E. Santamato, M. Romagnoli, M. Settembre, B. Daino, and Y. R. Shen, Phys. Rev. Lett. **61**, 113 (1988).
[5] L. Marrucci, G. Abbate, S. Ferraiuolo, P. Maddalena, and E. Santamato, Phys. Rev. A **46**, 4859 (1992).
[6] E. Brasselet, B. Doyon, T. V. Galstian, and L. J. Dube, Phys. Lett. A **299**, 212 (2002).
[7] E. Brasselet, B. Doyon, T. V. Galstian, and L. J. Dube, Phys. Rev. E **67**, 031706 (2003).
[8] D. O. Krimer, G. Demeter, and L. Kramer, Mol. Cryst. Liq. Cryst. **421**, 117 (2004).
[9] E. Brasselet, T. V. Galstian, L. J. Dube, D. O. Krimer, and L. Kramer, J. Opt. Soc. Am. B (to be published).
[10] E. Brasselet, B. Doyon, T. V. Galstian, and L. J. Dube, Phys. Rev. E **69**, 021701 (2004).
[11] P. G. de Gennes and J. Prost, *The Physics of Liquid Crystals* (Clarendon Press, Oxford, 1993).
[12] L. Marrucci, G. Abbate, S. Ferraiuolo, P. Maddalena, and E. Santamato, Mol. Cryst. Liq. Cryst. Sci. Technol., Sect. A **237**, 39 (1993).
[13] D. W. Berreman, J. Appl. Phys. **46**, 3746 (1975).
[14] C. Z. van Doorn, J. Appl. Phys. **46**, 3738 (1975).
[15] S. A. Jewell and J. R. Sambles, Appl. Phys. Lett. **82**, 3156 (2003).
[16] S. A. Jewell and J. R. Sambles, Appl. Phys. Lett. **84**, 46 (2004).
[17] V. Popa-Nita and P. Oswald, Phys. Rev. E **68**, 061707 (2003).
[18] F. M. Leslie, Q. J. Mech. Appl. Math. **19**, 357 (1966).
[19] O. Parodi, J. Phys. (Paris) **31**, 581 (1970).
[20] B. L. Winkler, H. Richter, I. Rehberg, W. Zimmermann, L. Kramer, and A. Buka, Phys. Rev. A **43**, 1940 (1991).
[21] E. Guyon, R. Meyer, and J. Salan, Mol. Cryst. Liq. Cryst. **54**, 261 (1979).
[22] A. Buka and L. Kramer, *Pattern Formation in Liquid Crystals* (Springer, Berlin, 1995).
[23] M. Abramowitz and I. A. Stegun, *Handbook of Mathematical Functions* (Dover, New York, 1970).
[24] E. Santamato, G. Abbate, P. Maddalena, L. Marrucci, and Y. R. Shen, Phys. Rev. Lett. **64**, 1377 (1990).
[25] A. Vella, B. Piccirillo, and E. Santamato, Phys. Rev. E **65**, 031706 (2002).
[26] D. O. Krimer, L. Kramer, E. Brasselet, T. V. Galstian, and L. J. Dube, J. Opt. Soc. Am. B (to be published).
[27] Refractive indices measured at 20 °C and $\lambda = 589$ nm from Merck datasheet.
[28] S. D. Durbin, S. M. Arakelian, and Y. R. Shen, Opt. Lett. **6**, 411 (1981).
[29] P. Glendinning, *Stability, Instability and Chaos* (Cambridge University Press, Cambridge, 1996).
[30] Istvan Janossy, J. Nonlinear Opt. Phys. Mater. **8**, 361 (1999).
[31] L. Marrucci, D. Paparo, P. Maddalena, E. Massera, E. Prudnikova, and E. Santamato, J. Chem. Phys. **107**, 9783 (1997).
[32] J. H. Huh, Y. Yusuf, Y. Hidaka, and S. Kai, Phys. Rev. E **66**, 031705 (2002).
[33] E. Santamato and Y. R. Shen, J. Opt. Soc. Am. A **4**, 356 (1987).